Supplementary material

Implementation

The algorithms presented here were implemented using Python 3.8 with PyTorch 2.3 and PyTorch Lightning 2.2. Moreover, MLflow 2.1 was utilised to perform experiment tracking.

Reconstruction performance metrics

Let us start by establishing some notation. We define the mean squared deviation (MSD) between two (static) shapes $\mathbf{s}_i = [\mathbf{x}_{i1}\ \mathbf{x}_{i2} ... \mathbf{x}_{iM}] \in \mathbb{R}^{3M}$ with $i = 1, 2$. The mean is taken across the M vertices, that is

$$\text{MSD}(\mathbf{s}_1, \mathbf{s}_2) := (1/M) \sum_{j=1}^{M} ||\mathbf{x}_{j2} - \mathbf{x}_{j2}||_2^2$$

Let us also define the temporal mean across the cycle, $\langle \cdot \rangle$:

$$\langle \mathbf{f} \rangle := \int_0^1 \mathbf{f}(t) dt. \tag{9}$$

where $0 \equiv 1 \equiv$ ED.

Our metrics are the following: $\varepsilon_s(t)$, which represents

$$\varepsilon_s(t) = \frac{\sum_{i=1}^{N_{\text{test}}} \text{MSD}\Big(\mathbf{s}_i(t), \hat{\mathbf{s}}_i(t)\Big)}{\sum_{i=1}^{N_{\text{test}}} \text{MSD}\Big(\mathbf{s}_i(t), \langle \mathbf{s}_i \rangle\Big)}. \tag{10}$$

On the other hand, the fraction of the style variation can be defined likewise:

$$\varepsilon_c(t) = \frac{\sum_i \text{MSD}\Big(\mathbf{s}_i(t), \hat{\mathbf{s}}_i(t)\Big)}{\sum_i \text{MSD}\Big(\mathbf{s}_i(t), \langle \mathbf{S} \rangle\Big)}, \tag{11}$$

$$\varepsilon_c = \frac{\sum_i \text{MSD}\Big(\langle \mathbf{s}_i(t) \rangle, \langle \hat{\mathbf{s}}_i(t) \rangle\Big)}{\sum_i \text{MSD}\Big(\langle \mathbf{s}_i \rangle, \langle \mathbf{S} \rangle\Big)}, \tag{12}$$

Finally, we define the time-averaged counterparts of the above quantities, $\langle \varepsilon_{s(c)} \rangle = \int_0^1 \varepsilon_{s(c)}(t) dt$.

Simulation of 3D meshes with periodic movement

To test our algorithm, we built a synthetic dataset consisting of meshes with a periodic time-dependent deformation parameterised in terms of spherical harmonics $Y_{lm}(\theta, \phi)$. We encoded content as well as style features. Among the advantages of using a synthetic dataset is the fact that these content and style factors (in particular, the complexity of the population) can be adjusted as desired.

Since the underlying content and style factors are known, it is possible to determine to what extent the retrieved latent factors resemble the real ones. We assess the linear identifiability of these variables (i.e. their correspondence up

to a linear transformation), by means of canonical correlation analysis (CCA). The results are shown in Supplementary Material and prove that the proposed network is effective in retrieving disentangled content and style latent factors.

Spherical harmonics. Spherical harmonics are the eigenfunctions of the Laplacian operated on the sphere, i.e. they satisfy the following equation:

$$\nabla^2 Y_{lm}(\theta, \phi) = l(l+1) Y_{lm}(\theta, \phi) \tag{13}$$

The explicit formula for these functions is the following:

$$Y_{lm}(\theta, \phi) = N_{lm} P_l^m(\cos\theta) e^{im\phi}, \tag{14}$$

where P_l^m are the associated Legendre polynomials and $N_{lm} = \sqrt{\frac{(2l+1)}{4\pi} \frac{(l+m)!}{l-m)!}}$ is a normalization constant, that ensure the polynomials constitute an orthonormal basis, that is

$$\int_0^\pi \int_0^\pi Y_{lm}(\theta, \phi) Y^*_{l'm'}(\theta, \phi) d\theta d\phi = \delta_{ll'} \delta_{mm'}$$

The deformation with respect to the reference spherical shape is performed in the radial direction at each location, as a linear combination of the Y_{lm} with $l = 0, ..., l_{\text{max}}$ and $m = -l, -l+1, ..., l.$. Since a complex-valued deformation does not make sense for our case, we use the real counterparts of these functions, where: Y

Generative model. The generative model used was the following:

$$b_{lm}^{(0)} \overset{\text{i.i.d}}{\sim} \mathcal{N}(0, \sigma_c^2)$$

$$a_{lm}^{(n)}, b_{lm}^{(n)} \overset{\text{i.i.d}}{\sim} \mathcal{N}(0, \sigma_s^2), n \geq 1$$

With these coefficients, time-periodic coefficients are generated for each Y_{lm}. To make the deformation periodic in time, we build the coefficients as a linear combination of sines and cosines functions, with frequencies n that are multiples of the fundamental frequency, taken to be the unit:

$$a_{lm}(t) = b_{lm}^{(0)} + \sum_{n=1}^{n_{\text{max}}} \left[a_{lm}^{(n)} \sin(2\pi n t) + b_{lm}^{(n)} \cos(2\pi n t) \right]$$

Finally, the shape at time t is given by the following:

$$\mathbf{d}(\theta, \phi, t) = \left(\sum_{l=0}^{l_{\text{max}}} \sum_{m=-l}^{l} a_{lm}(t) Y_{lm}(\theta, \phi) \right) \hat{\mathbf{r}}(\theta, \phi)$$

where $\hat{\mathbf{r}}(\theta, \phi)$ is a unit vector in the radial direction (i.e. the deformations are performed along the radial direction).

Therefore, the population is completely defined by N, l_{max}, σ_c^2, σ_s^2 and a random seed s. The complexity of the population of meshes is given by the number of latent factors C, which in turn is determined by l_{max} and n_{max}; in particular, $C = (l_{\text{max}} + 1)^2 (n_{\text{max}} + 1)$, from which $C_c = (l_{\text{max}} + 1)^2$ correspond to content and $C_s = (l_{\text{max}} + 1)^2 n_{\text{max}}$ correspond to style. For example, with $l_{\text{max}} = n_{\text{max}} = 2$, we get $C = C_c + C_s = 9 + 18 = 27$.

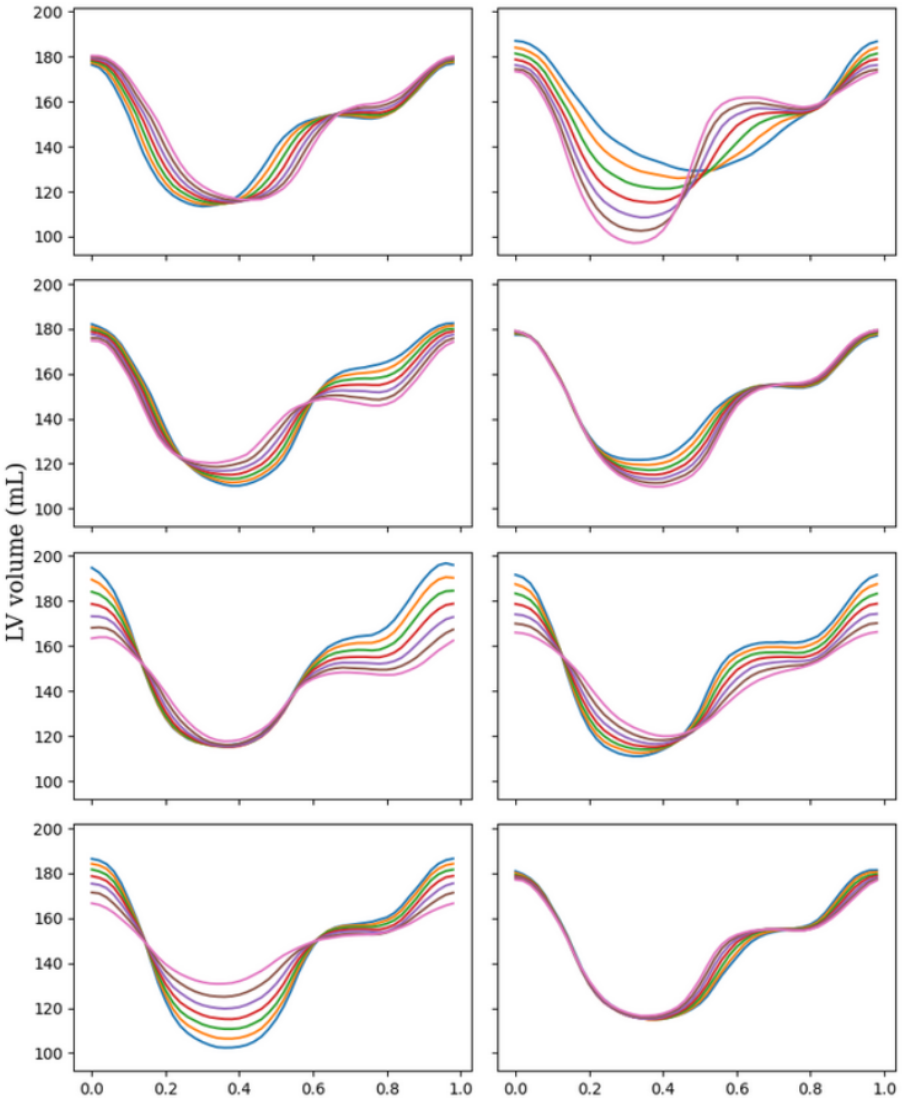

Figure S1: Volume curves for synthetic LV shapes obtained by varying each of the eight dynamic latent variables one at a time.

Traversals for an LV run with $n_z^{(s)} = 8$

Figure S1 shows the volume curves traversals for all the 8 dynamic latent embeddings, for a single run on LV.

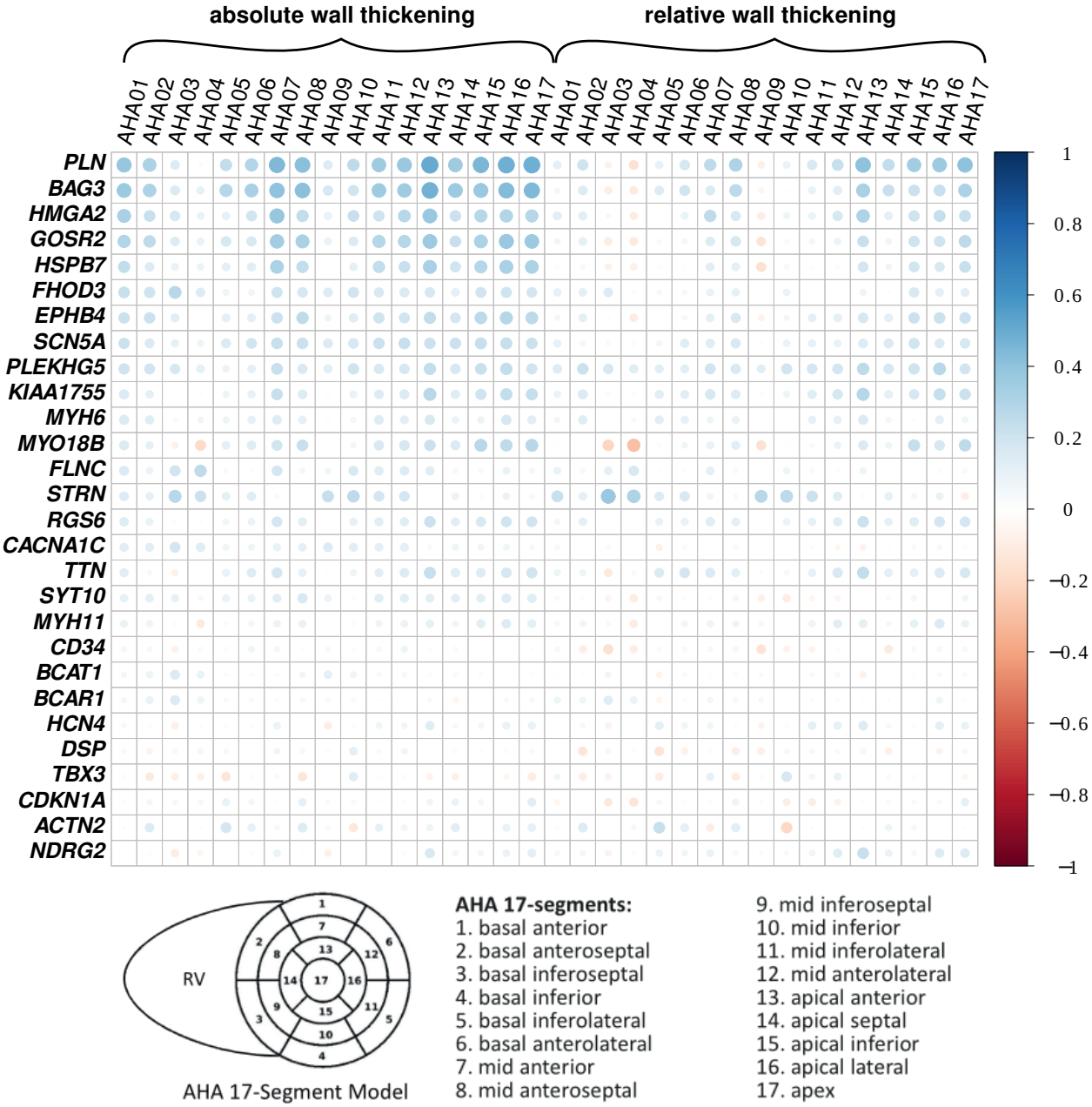

Figure S2: a) correlation between best latent variable per locus and absolute and relative wall thickening per AHA segment and b) the 17 AHA LV segments.

LLM prompt for gene prioritization

5.6.1 Gene prioritisation via Large Language Models (LLMs)

Following previous work which suggests that LLMs have the capacity to help in identifying candidate genes [33], in order to identify candidate genes for each locus, the following procedure was carried out: for each lead variant, a 1Mb

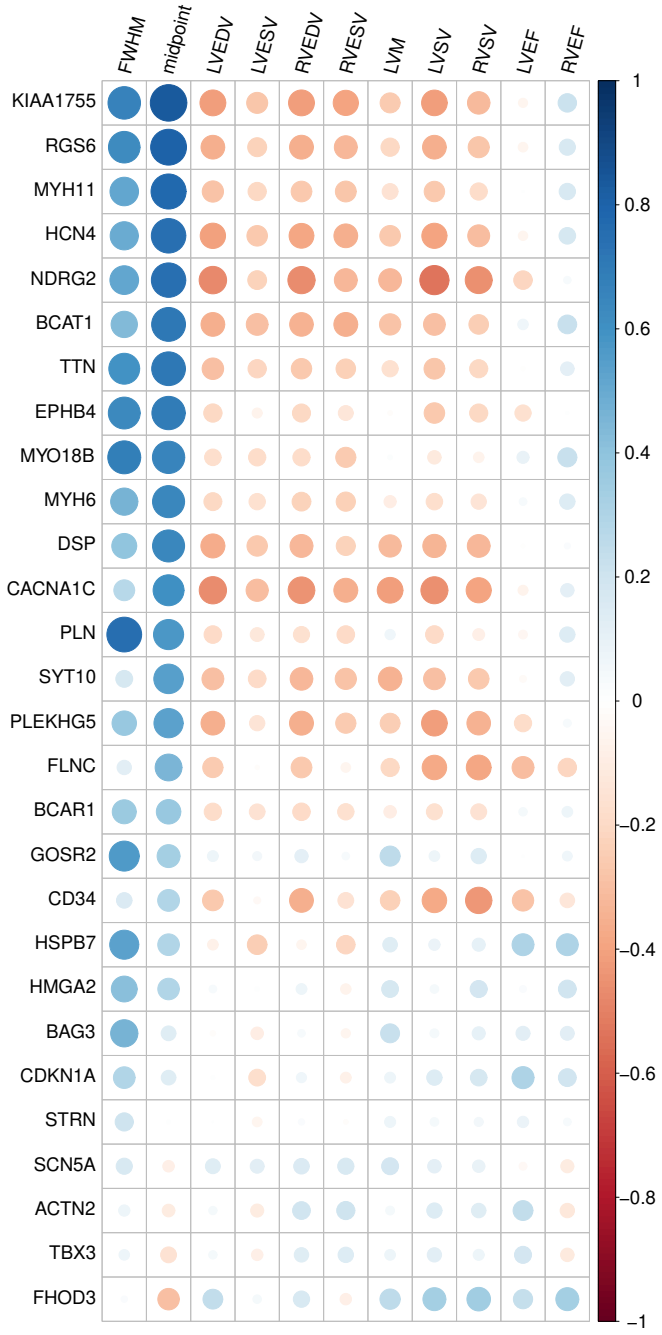

Figure S3: Spearman correlation between the best latent variable per locus and several handcrafted indices.

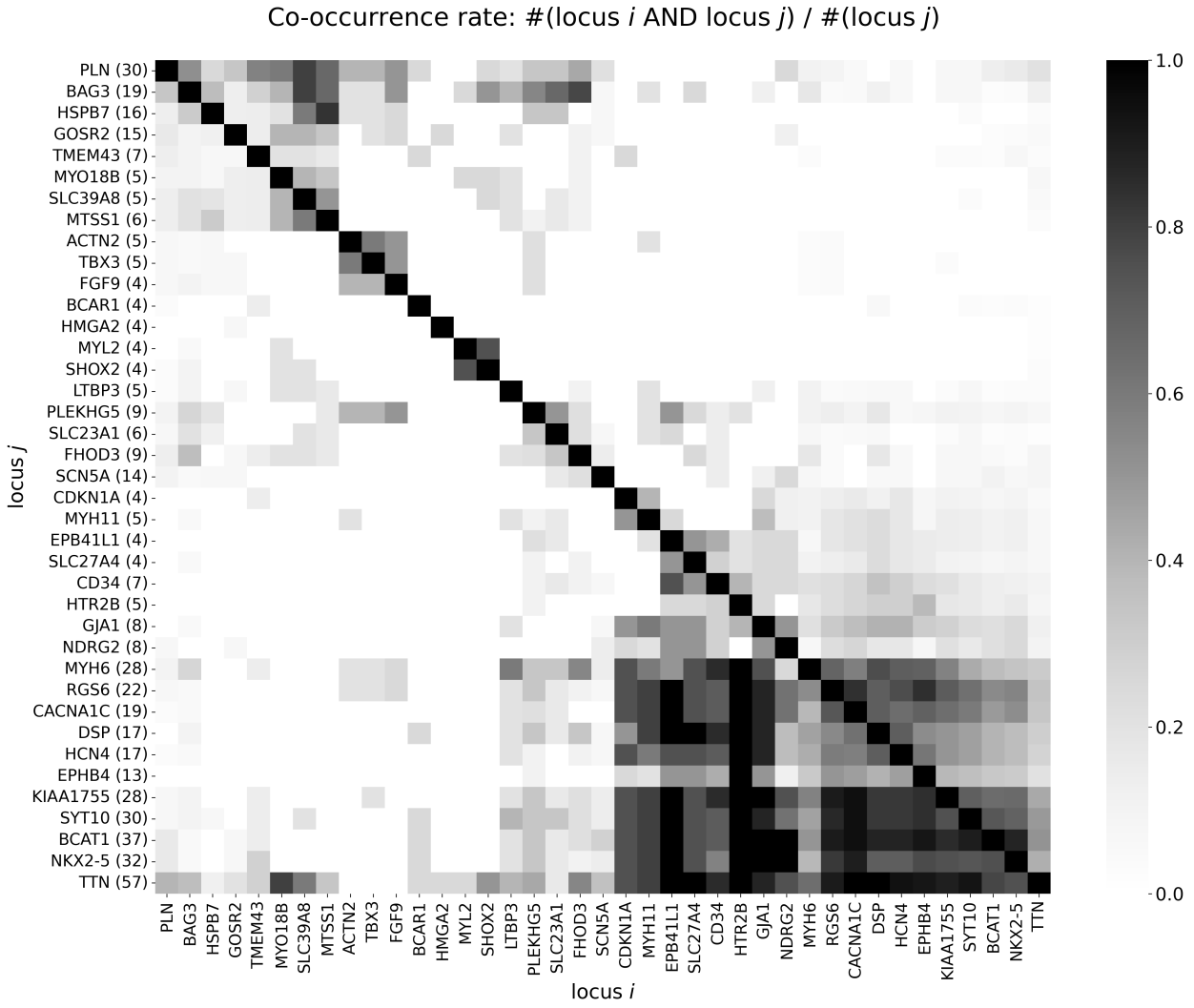

Figure S4: Heatmap depicting the GWAS hit *co-occurrence matrix*: intensity of the gray colour indicates the fraction of times that the locus in the row is detected with $p < p_{\text{GW}}$, given that the locus in the columns is also detected with $p < p_{\text{GW}}$. The number between parenthesis after the locus name indicates how many times this locus was discovered in total. For instance, locus *NKX2-5* is detected 32 times (i.e. for 32 different latent variables) and almost always ($f = 0.94$) the locus *HTR2B* is also detected with genome-wide significance. However, loci such as *ACTN2*, *TBX3*, *FGF9* and *MYL2* (among others) are never detected alongside the previous loci.

Source	Term name	p-value	Intersection size	Term size
GO:BP	heart development	1.1×10^{-4}	11	600
HP	Thromboembolic stroke	1.7×10^{-4}	6	74
HP	Atrial fibrillation	3.8×10^{-4}	6	84
HP	Atrial arrhythmia	6.5×10^{-4}	6	92
HP	Thromboembolism	1.1×10^{-3}	6	100
GO:BP	circulatory system development	1.3×10^{-3}	13	1134
GO:BP	cardiac muscle cell development	1.5×10^{-3}	5	79
HP	Orthopnea	1.5×10^{-3}	6	106
GO:BP	cardiocyte differentiation	1.7×10^{-3}	6	150
GO:BP	cardiac cell development	2.1×10^{-3}	5	85
GO:CC	Z disc	2.7×10^{-3}	5	134
GO:BP	striated muscle cell development	2.8×10^{-3}	6	164
GO:CC	actin cytoskeleton	3.8×10^{-3}	8	516
GO:CC	myosin filament	4.1×10^{-3}	3	23
GO:CC	I band	4.6×10^{-3}	5	149
HP	Supraventricular arrhythmia	5.7×10^{-3}	6	133
GO:CC	myosin II complex	6.0×10^{-3}	3	26
GO:BP	adult heart development	6.2×10^{-3}	3	14
GO:BP	muscle cell development	6.8×10^{-3}	6	191
HP	Tricuspid regurgitation	7.2×10^{-3}	5	77
HP	Lipoatrophy	7.6×10^{-3}	5	78
HP	Abnormal EKG	8.1×10^{-3}	6	141
GO:BP	atrioventricular node cell fate commitment	8.2×10^{-3}	2	2
HP	Abnormal tricuspid valve physiology	8.7×10^{-3}	5	80
HP	Exertional dyspnea	8.7×10^{-3}	6	143

Table S1: Top 25 enriched terms from g:Profiler analysis.

window was established centred on the variant and genes within that window were used to build an LLM query. The query included a request to order the genes from the most likely to the least likely to be causative of the association. The query output was manually curated and cross-referenced with genomic proximity information to further prioritise the proposed genes. The prompt utilised was the following: "Act as a cardiac geneticist. Out of the following list of genes, which of them are expected to have a role in a cardiac phenotype: `<gene list>`? Order them from most likely to least likely, providing the supporting evidence." Here, `<gene list>` corresponds to all protein-coding genes located within a 1 Mb window centered on the lead variant.

We combined this language-model-derived prioritisation with positional proximity, giving highest priority to genes that were both close to the lead SNP and supported by prior evidence as identified by the model. This hybrid approach integrates automated biomedical knowledge retrieval with traditional locus-centric prioritisation.

Results for each chamber and variable type

Tables S2 through S9 show results for the different cardiac chambers, except for LV which is shown in the main text.

chr.	region	candidate gene	count	min. p-value	SNP	NEA	EA	EAF	$\hat{\beta} \pm \text{se}(\hat{\beta})(\times 100)$
6	117672972-118963115	PLN	5	6.2×10^{-16}	rs12661338	C	A	44.9	-5.67 ± 0.7
17	43056905-45876022	GOSR2	5	1.1×10^{-13}	rs17677363	A	T	13.2	8.41 ± 1.01
2	178553183-181312739	TTN	5	1.9×10^{-12}	rs10497529	G	A	3.6	-7.78 ± 1.84
12	110336719-113263518	MYL2	4	2.7×10^{-15}	rs35350651	A	AC	51.4	-2.77 ± 0.69
1	14891511-16897730	HSPB7	4	2.1×10^{-12}	rs1627145	C	T	65.7	5.13 ± 0.73
3	99373762-100592217	FILIP1L	3	1.1×10^{-09}	rs9865713	G	A	37.9	3.37 ± 0.72
2	36122006-38132712	STRN	3	2.2×10^{-10}	rs2013223	T	C	58.7	-4.26 ± 0.67
10	120591353-122407323	BAG3	3	9.2×10^{-11}	rs72840788	G	A	21.5	-5.52 ± 0.85
14	23018665-24905123	MYH6	3	3.7×10^{-11}	rs376439	A	G	39.5	-2.34 ± 0.68
3	157312028-159477890	SHOX2	3	8.2×10^{-12}	rs56148815	G	C	40.1	4.42 ± 0.74
12	27799773-29651255	CCDC91	3	8.9×10^{-14}	12:28491249_GT_G	GT	G	25.9	6.03 ± 0.81
16	4001196-5118345	SRL	2	3.7×10^{-10}	rs868302	A	G	23.5	4.71 ± 0.83
13	93586455-96087558	DCT	2	4.3×10^{-10}	rs9524217	G	A	29.6	-4.75 ± 0.76
7	118351581-121045273	WNT16	2	1.2×10^{-09}	rs3779381	A	G	26.3	2.87 ± 0.79
15	48136048-50008043	FBN1	2	6.2×10^{-09}	rs61999107	C	T	10.3	5.31 ± 1.17
18	33861964-35075250	FHOD3	2	6.6×10^{-09}	rs34617432	C	CA	27.1	2.79 ± 0.8
5	171074292-172678327	NKX2-5	1	1.1×10^{-10}	rs6882776	G	A	28.6	-3.14 ± 0.78

Table S2: GWAS results for static variables for RV.

chr.	region	candidate gene	count	min. p-value	SNP	NEA	EA	EAF	$\hat{\beta} \pm \text{se}(\hat{\beta})(\times 100)$
2	178553183-181312739	TTN	5	4.4×10^{-18}	rs17362588	G	A	8.7	8.61 ± 1.21
14	23018665-24905123	MYH6	5	1.7×10^{-13}	rs365990	A	G	36.9	4.22 ± 0.72
12	23820634-25371083	BCAT1	4	3.8×10^{-23}	rs4963772	G	A	15.0	-5.9 ± 0.97
5	171074292-172678327	NKX2-5	4	3.2×10^{-18}	5:172643468_GC_G	GC	G	16.4	6.15 ± 0.96
20	34960446-36909530	KIAA1755	4	3.9×10^{-17}	rs2881138	A	G	46.2	-3.09 ± 0.7
12	33076989-37856717	SYT10	4	5.4×10^{-15}	rs11052736	T	C	45.6	3.13 ± 0.7
15	73628714-76398624	HCN4	4	1.1×10^{-12}	rs7172796	T	G	15.9	-6.77 ± 0.95
6	6785207-7808936	DSP	4	1.5×10^{-09}	rs72825054	G	C	9.7	7.15 ± 1.18
14	71131957-72889615	RGS6	4	4.0×10^{-12}	rs17180489	G	C	14.5	4.3 ± 0.93
12	1080331-2544786	CACNA1C	4	1.3×10^{-11}	rs2283274	G	C	17.8	-4.32 ± 0.92
7	100196651-101199253	EPHB4	3	2.9×10^{-10}	rs9691107	T	C	40.2	-3.62 ± 0.72
3	157312028-159477890	SHOX2	3	8.9×10^{-09}	rs6792449	T	C	50.2	-2.82 ± 0.71
4	100678360-103221356	SLC39A8	3	1.4×10^{-09}	rs35225200	A	C	7.9	5.68 ± 1.32
10	120591353-122407323	BAG3	3	7.0×10^{-10}	rs2234962	T	C	21.5	-5.49 ± 0.84
14	19002084-21589402	NDRG2	3	3.4×10^{-10}	rs12889267	A	G	16.7	-3.97 ± 0.93
1	14891511-16897730	HSPB7	3	1.0×10^{-10}	rs12744578	A	T	28.6	3.6 ± 0.77
17	43056905-45876022	GOSR2	3	1.5×10^{-10}	rs1358071	C	A	73.5	-4.9 ± 0.78
6	117672972-118963115	PLN	3	6.1×10^{-19}	rs3951016	T	A	47.1	-6.23 ± 0.7
6	120512128-121905676	GJA1	3	1.0×10^{-11}	rs34782269	G	GA	50.1	2.99 ± 0.71
3	38356116-40221298	SCN5A	3	6.4×10^{-14}	rs6795970	A	G	60.3	-5.33 ± 0.71
8	125683719-126410917	MTSS1	2	1.9×10^{-11}	8:125858538_GA_G	GA	G	31.0	3.07 ± 0.76
22	24984204-26791628	MYO18B	2	1.0×10^{-09}	rs133890	C	G	45.2	-3.42 ± 0.7
11	63804569-65898631	LTBP3	2	9.6×10^{-09}	rs2096560	T	C	23.5	4.74 ± 0.82
3	13070799-14816900	TMEM43	2	1.5×10^{-08}	rs73133428	C	T	18.5	4.97 ± 0.88
2	231843389-233550003	HTR2B	2	2.3×10^{-08}	rs12993290	G	A	22.1	-4.14 ± 0.84
9	126971887-129059665	chr9_64	2	2.5×10^{-08}	rs473426	G	C	54.0	3.89 ± 0.7
12	110336719-113263518	MYL2	2	3.1×10^{-08}	rs58235019	A	AG	60.5	-3.91 ± 0.71
1	235819436-237555628	ACTN2	1	2.9×10^{-10}	rs4659701	G	A	62.2	2.93 ± 0.73
12	115036602-115503216	TBX3	1	2.2×10^{-12}	rs7309382	T	C	40.2	2.57 ± 0.71

Table S3: GWAS results for dynamic variables for RV.

chr.	region	candidate gene	count	min. p-value	SNP	NEA	EA	EAF	$\hat{\beta} \pm \text{se}(\hat{\beta})(\times 100)$
6	117672972-118963115	PLN	5	8.2×10^{-27}	rs72967533	T	C	47.7	5.29 ± 0.7
12	110336719-113263518	MYL2	5	8.7×10^{-17}	rs35350651	A	AC	51.4	-2.77 ± 0.69
2	178553183-181312739	TTN	5	2.5×10^{-17}	rs10497529	G	A	3.6	-7.78 ± 1.84
1	14891511-16897730	HSPB7	5	2.8×10^{-14}	rs1763619	A	G	65.7	-4.67 ± 0.73
14	23018665-24905123	MYH6	5	7.9×10^{-13}	rs365990	A	G	36.9	4.22 ± 0.72
10	120591353-122407323	BAG3	5	1.1×10^{-12}	rs72840788	G	A	21.5	-5.52 ± 0.85
3	13070799-14816900	TMEM43	5	6.8×10^{-12}	rs73028848	A	G	34.0	5.08 ± 0.74
3	157312028-159477890	SHOX2	5	1.5×10^{-11}	rs56148815	G	C	40.1	4.42 ± 0.74
4	119933512-120392684	MYOZ2	4	6.3×10^{-10}	rs28634456	A	G	29.9	-4.73 ± 0.77
2	36122006-38132712	STRN	3	4.3×10^{-11}	rs2110944	T	C	52.6	-4.04 ± 0.7
16	4001196-5118345	SRL	3	2.3×10^{-09}	rs868302	A	G	23.5	4.71 ± 0.83
1	226810860-229156248	OBSCN	3	9.0×10^{-09}	rs883748	C	T	47.6	2.94 ± 0.66
7	118351581-121045273	WNT16	3	7.0×10^{-15}	rs3779381	A	G	26.3	2.87 ± 0.79
17	43056905-45876022	GOSR2	3	1.0×10^{-15}	rs17677363	A	T	13.2	8.41 ± 1.01
17	67858770-69387817	KCNJ2	2	6.5×10^{-09}	rs180063	A	G	25.8	-3.46 ± 0.84
6	125424383-127540461	HEY2	2	2.7×10^{-09}	rs373980643	GT	G	46.0	3.22 ± 0.7
3	99373762-100592217	FILIP1L	2	2.0×10^{-09}	rs7636776	T	C	41.2	4.24 ± 0.71
3	72529329-74321817	PDZRN3	2	6.7×10^{-10}	rs7631905	C	T	47.3	4.14 ± 0.7
6	1452362-2458936	GMDS	2	3.9×10^{-08}	rs6934958	T	C	54.9	2.87 ± 0.7
12	113986709-115036602	TBX5	2	4.2×10^{-10}	rs1895606	C	T	46.5	2.86 ± 0.7
16	74971503-75977954	BCAR1	2	8.4×10^{-11}	rs12446877	T	C	62.7	3.75 ± 0.72
12	27799773-29651255	CCDC91	2	1.1×10^{-11}	rs10843115	C	T	27.4	5.31 ± 0.78
14	19002084-21589402	NDRG2	1	4.6×10^{-10}	rs12889267	A	G	16.7	-3.97 ± 0.93
17	63148128-64800430	PRKCA	1	2.9×10^{-10}	rs9892651	C	T	58.1	4.46 ± 0.71
15	99244059-100636847	LRRC28	1	4.6×10^{-11}	rs2871974	C	T	63.5	3.68 ± 0.73
1	182755356-184595513	SMG7	1	7.7×10^{-11}	rs789185	A	G	39.3	-3.42 ± 0.72

Table S4: GWAS results for static variables for BV.

chr.	region	candidate gene	count	min. p-value	SNP	NEA	EA	EAF	$\hat{\beta} \pm \text{se}(\hat{\beta})(\times 100)$
14	23018665-24905123	MYH6	5	3.7×10^{-17}	rs422068	T	C	35.9	-3.25 ± 0.72
20	34960446-36909530	KIAA1755	5	3.3×10^{-15}	rs2881138	A	G	46.2	-3.09 ± 0.7
3	38356116-40221298	SCN5A	5	8.4×10^{-11}	rs6783110	A	G	59.9	4.64 ± 0.71
5	171074292-172678327	NKX2-5	5	5.8×10^{-17}	5:172643468_GC_G	GC	G	16.4	6.15 ± 0.96
14	71131957-72889615	RGS6	5	9.5×10^{-12}	rs17180489	G	C	14.5	4.3 ± 0.93
10	120591353-122407323	BAG3	5	1.5×10^{-12}	rs72840788	G	A	21.5	-5.52 ± 0.85
12	33076989-37856717	SYT10	5	1.7×10^{-14}	12:33654815_CA_C	CA	C	54.3	-3.74 ± 0.7
12	23820634-25371083	BCAT1	5	9.6×10^{-17}	rs4963772	G	A	15.0	-5.9 ± 0.97
6	117672972-118963115	PLN	5	7.6×10^{-17}	rs72967533	T	C	47.7	5.29 ± 0.7
2	178553183-181312739	TTN	5	7.3×10^{-17}	rs17362588	G	A	8.7	8.61 ± 1.21
18	33861964-35075250	FHOD3	4	8.1×10^{-15}	rs2644262	T	C	27.5	4.67 ± 0.78
12	115036602-115503216	TBX3	4	6.2×10^{-14}	rs7300371	T	C	73.1	4.56 ± 0.79
12	1080331-2544786	CACNA1C	4	6.8×10^{-12}	rs2283274	G	C	17.8	-4.32 ± 0.92
1	14891511-16897730	HSPB7	4	1.0×10^{-09}	1:16141512_CTTT_C	CTTT	C	37.6	3.04 ± 0.69
1	5913893-7247335	PLEKHG5	4	7.0×10^{-10}	1:6283547_GA_G	GA	G	15.2	-5.87 ± 0.99
17	43056905-45876022	GOSR2	3	3.7×10^{-10}	rs1358071	C	A	73.5	-4.9 ± 0.78
14	19002084-21589402	NDRG2	3	2.0×10^{-09}	rs12889267	A	G	16.7	-3.97 ± 0.93
6	6785207-7808936	DSP	3	1.2×10^{-11}	rs6920534	T	C	9.9	8.0 ± 1.18
1	235819436-237555628	ACTN2	3	2.1×10^{-15}	rs12724121	A	T	62.2	-2.56 ± 0.68
13	20686720-22242174	FGF9	3	2.2×10^{-08}	rs4990057	C	T	42.8	2.96 ± 0.71
15	73628714-76398624	HCN4	2	8.4×10^{-10}	rs11630367	A	G	15.8	-4.83 ± 0.95
22	24984204-26791628	MYO18B	2	9.1×10^{-10}	rs133885	G	A	45.2	-3.21 ± 0.7
1	206073265-208410364	CD34	2	1.4×10^{-10}	rs861475	T	C	53.0	2.62 ± 0.71
5	136376050-139265072	SLC23A1	2	1.3×10^{-08}	rs74803899	T	C	5.5	7.46 ± 1.53
12	113986709-115036602	TBX5	2	1.4×10^{-08}	rs883079	C	T	72.9	3.71 ± 0.79
3	168580960-170964909	SAMD7*	1	3.2×10^{-10}	rs11383131	A	AC	60.7	3.16 ± 0.71
4	174264132-176570716	HAND2	1	2.2×10^{-10}	rs10005540	C	T	61.7	2.99 ± 0.72

Table S5: GWAS results for dynamic variables for BV.

chr.	region	candidate gene	count	min. p-value	SNP	NEA	EA	EAF	$\hat{\beta} \pm \text{se}(\hat{\beta})(\times 100)$
4	111256567-113870102	PITX2	4	7.7×10^{-09}	rs2723321	A	G	69.6	-4.4 ± 0.76
2	178553183-181312739	TTN	3	2.3×10^{-14}	rs17362588	G	A	8.7	8.61 ± 1.21
17	43056905-45876022	GOSR2	3	1.8×10^{-11}	rs533030436	A	G	11.8	5.07 ± 1.12
4	100678360-103221356	SLC39A8	2	1.2×10^{-09}	rs13107325	C	T	7.0	-5.29 ± 1.35
2	54685226-56203345	EFEMP1	2	10.0×10^{-09}	rs147444949	A	G	1.3	11.26 ± 2.86

Table S6: GWAS results for static variables for LA.

chr.	region	candidate gene	count	min. p-value	SNP	NEA	EA	EAF	$\hat{\beta} \pm \text{se}(\hat{\beta})(\times 100)$
2	178553183-181312739	TTN	5	1.6×10^{-15}	rs17362588	G	A	8.7	8.61 ± 1.21
5	171074292-172678327	NKX2-5	5	5.4×10^{-12}	rs11134777	G	T	16.5	-6.56 ± 0.95
6	117672972-118963115	PLN	5	1.9×10^{-11}	rs72967533	T	C	47.7	5.29 ± 0.7
12	23820634-25371083	BCAT1	3	3.9×10^{-18}	rs4963772	G	A	15.0	-5.9 ± 0.97
7	100196651-101199253	EPHB4	3	2.4×10^{-10}	rs2720392	C	A	49.6	3.11 ± 0.7
16	74971503-75977954	BCAR1	3	2.8×10^{-16}	rs59686216	A	G	60.0	3.79 ± 0.72
14	23018665-24905123	MYH6	3	6.5×10^{-15}	rs365990	A	G	36.9	4.22 ± 0.72
12	33076989-37856717	SYT10	3	3.0×10^{-14}	rs11052736	T	C	45.6	3.13 ± 0.7
12	1080331-2544786	CACNA1C	3	3.6×10^{-13}	rs2283274	G	C	17.8	-4.32 ± 0.92
14	71131957-72889615	RGS6	3	2.8×10^{-12}	rs17180489	G	C	14.5	4.3 ± 0.93
12	65559695-67181144	HMGA2	3	1.5×10^{-08}	rs761210718	AAG	A	36.9	-3.14 ± 0.72
20	34960446-36909530	KIAA1755	3	9.4×10^{-17}	rs2881138	A	G	46.2	-3.09 ± 0.7
1	14891511-16897730	HSPB7	2	1.9×10^{-09}	rs12138117	T	C	32.2	-4.45 ± 0.74
6	120512128-121905676	GJA1	2	9.2×10^{-10}	rs34782269	G	GA	50.1	2.99 ± 0.71
15	73628714-76398624	HCN4	2	7.9×10^{-10}	rs11630367	A	G	15.8	-4.83 ± 0.95
16	14464002-16154060	MYH11	2	4.5×10^{-11}	rs9284324	G	A	32.0	-3.25 ± 0.76
18	33861964-35075250	FHOD3	2	2.3×10^{-10}	rs2848901	C	T	28.5	3.45 ± 0.77
10	120591353-122407323	BAG3	2	1.4×10^{-10}	rs7095308	G	A	27.5	4.42 ± 0.78
17	43056905-45876022	GOSR2	2	1.2×10^{-10}	rs76774446	C	A	13.2	-6.16 ± 1.02
6	6785207-7808936	DSP	2	1.2×10^{-10}	rs6920534	T	C	9.9	8.0 ± 1.18
3	13070799-14816900	TMEM43	2	2.2×10^{-08}	rs73031103	A	G	34.0	4.33 ± 0.74
7	126869221-128778386	FLNC	1	4.7×10^{-12}	rs4472439	G	A	11.2	7.65 ± 1.11

Table S7: GWAS results for dynamic variables for LA.

chr.	region	candidate gene	count	min. p-value	SNP	NEA	EA	EAF	$\hat{\beta} \pm \text{se}(\hat{\beta})(\times 100)$
17	43056905-45876022	GOSR2	5	1.6×10^{-18}	rs11874	G	A	13.3	4.99 ± 1.01
12	27799773-29651255	CCDC91*	3	1.4×10^{-10}	rs200507341	C	CT	20.1	3.58 ± 0.89
2	178553183-181312739	TTN	2	2.4×10^{-12}	rs151041685	G	T	8.7	-7.0 ± 1.22
6	117672972-118963115	PLN	2	4.4×10^{-10}	rs11153730	T	C	48.6	3.8 ± 0.69
12	65559695-67181144	HMGA2	2	3.7×10^{-09}	rs761210718	AAG	A	36.9	-3.14 ± 0.72
14	23018665-24905123	MYH6	1	1.2×10^{-10}	rs422068	T	C	35.9	-3.25 ± 0.72

Table S8: GWAS results for static variables for RA.

chr.	region	candidate gene	count	min. p-value	SNP	NEA	EA	EAF	$\hat{\beta} \pm \text{se}(\hat{\beta})(\times 100)$
12	23820634-25371083	BCAT1	4	3.3×10^{-21}	rs4963772	G	A	15.0	-5.9 ± 0.97
2	178553183-181312739	TTN	4	4.3×10^{-18}	rs10497529	G	A	3.6	-7.78 ± 1.84
20	34960446-36909530	KIAA1755	4	8.1×10^{-16}	rs2881138	A	G	46.2	-3.09 ± 0.7
5	171074292-172678327	NKX2-5	4	6.2×10^{-15}	rs539079213	C	CT	15.5	-3.83 ± 1.02
12	33076989-37856717	SYT10	4	7.3×10^{-15}	rs11052736	T	C	45.6	3.13 ± 0.7
14	23018665-24905123	MYH6	3	4.9×10^{-12}	rs376439	A	G	39.5	-2.34 ± 0.68
6	6785207-7808936	DSP	3	3.0×10^{-09}	rs112019128	C	T	9.6	-6.23 ± 1.19
17	43056905-45876022	GOSR2	3	2.4×10^{-10}	rs9896243	C	G	21.0	5.37 ± 0.85
12	1080331-2544786	CACNA1C	3	1.5×10^{-10}	rs2283274	G	C	17.8	-4.32 ± 0.92
14	71131957-72889615	RGS6	3	1.8×10^{-12}	rs17180489	G	C	14.5	4.3 ± 0.93
3	38356116-40221298	SCN5A	3	1.4×10^{-19}	rs6801957	T	C	59.7	-3.92 ± 0.67
15	73628714-76398624	HCN4	3	1.2×10^{-12}	rs7172796	T	G	15.9	-6.77 ± 0.95
6	120512128-121905676	GJA1	2	2.8×10^{-10}	rs34782269	G	GA	50.1	2.99 ± 0.71
1	5913893-7247335	PLEKHG5	2	6.8×10^{-10}	rs796136824	GA	G	23.2	4.62 ± 0.93
6	117672972-118963115	PLN	2	1.1×10^{-12}	rs57912492	C	T	41.9	-2.9 ± 0.71
1	206073265-208410364	CD34	2	1.1×10^{-08}	rs2785647	G	A	34.3	3.95 ± 0.73
7	100196651-101199253	EPHB4	1	3.4×10^{-10}	rs9691107	T	C	40.2	-3.62 ± 0.72

Table S9: GWAS results for dynamic variables for RA.

Manhattan plots for handcrafted indices

Manhattan plots are shown in Figure S5 and S6 for GWAS on full-width at half maximum LVV (FWHM) and the time of minimum LVV (with a cardiac cycle normalised to [0,1]).

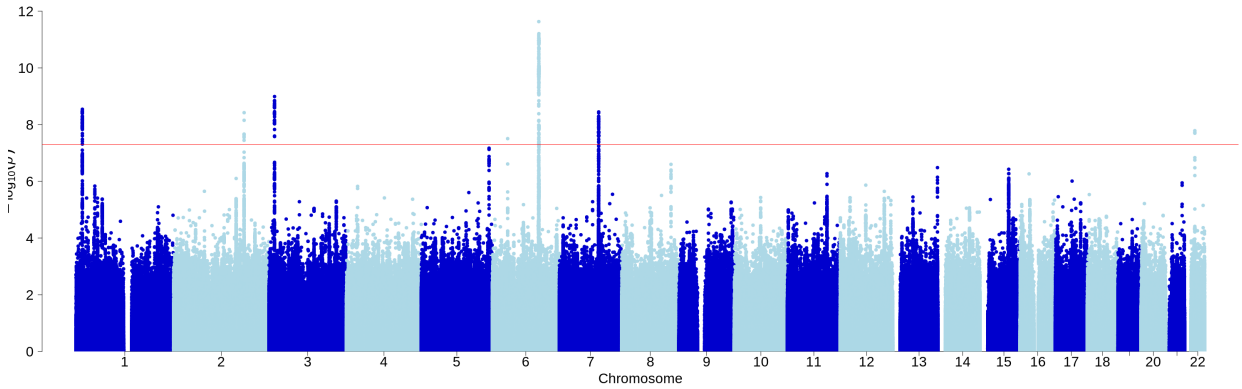

Figure S5: Manhattan plot for LVV FWHM: the temporal width between the instant at 50% contraction and the instant at 50% relaxation, as a fraction of the length of the cardiac cycle.

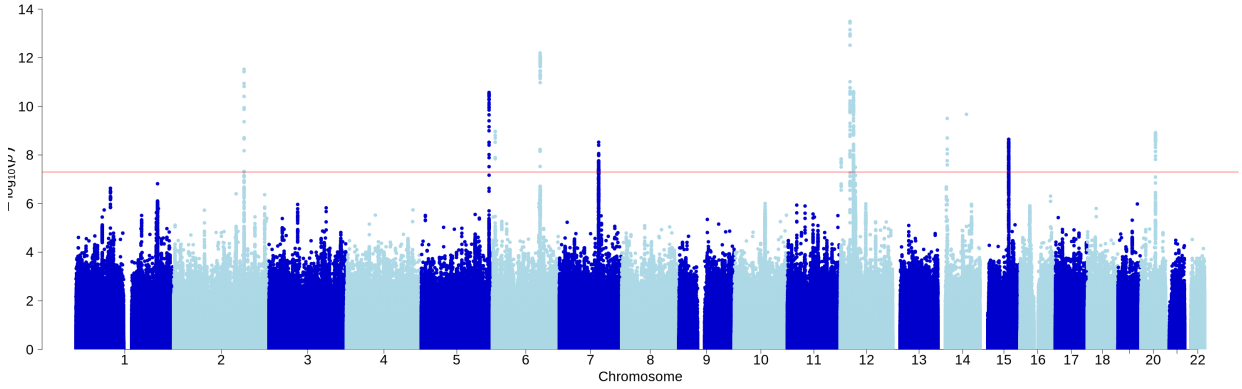

Figure S6: Manhattan plot for the position of the LVV minimum across the cardiac cycle (as a fraction of the length of the cycle).